

Article

Study Method of Pitch-Angle Control on Load and the Performance of a Floating Offshore Wind Turbine by Experiments

Le Quang Sang^{1,2}, Qing'an Li^{3,4}, Takao Maeda^{5,*}, Yasunari Kamada⁵, Duc Nguyen Huu⁶ , Quynh T. Tran^{1,7,*} 
and Eleonora Riva Sanseverino^{8,9} 

- ¹ Institute of Energy Science—Vietnam Academy of Science and Technology, 18 Hoang Quoc Viet, Nghia Do, Cau Giay, Hanoi 10072, Vietnam
 - ² Faculty of Materials and Energy Science, Graduate University of Science and Technology—Vietnam Academy of Science and Technology, 18 Hoang Quoc Viet, Cau Giay, Hanoi 10072, Vietnam
 - ³ CAS Laboratory of Wind Energy Utilization, Institute of Engineering Thermophysics, Chinese Academy of Sciences, Beijing 100190, China
 - ⁴ University of Chinese Academy of Sciences, Beijing 100049, China
 - ⁵ Division of Mechanical Engineering, Mie University, 1577 Kurimamachiya-cho, Tsu 514-8507, Mie, Japan
 - ⁶ Faculty of Energy Technology, Electric Power University, 235 Hoang Quoc Viet, Hanoi 11355, Vietnam
 - ⁷ Hawaii Natural Energy Institute, University of Hawaii at Manoa, Honolulu, HI 96822, USA
 - ⁸ Department of Engineering, University of Palermo, 90128 Palermo, Italy
 - ⁹ ENSIEL Consorzio Interuniversitario Nazionale “Energia e Sistemi Elettrici”, 50121 Firenze, Italy
- * Correspondence: maeda@mach.mie-u.ac.jp (T.M.); tranttq@hawaii.edu (Q.T.T.)

Abstract: Offshore wind energy is a renewable energy source that is developing fast. It is considered to be the most promising energy source in the next decade. Besides, the expanding trend for this technology requires the consideration of diversified seabeds. In deep seabeds, floating offshore wind technology (FOWT) is needed. For this latter technology, such as for conventional WT, we need to consider aspects related to performance, aerodynamic force, and forces during operation. In this paper, a two-bladed downwind wind turbine model is utilized to conduct experiments. The collective pitch and cyclic pitch angle are adjusted using swashplated equipment. The fluid forces and moments acting on the rotor surface are measured by a six-component balancing system. By changing the pitch angle of the wind turbine blades, attempts are made to manage the fluid forces generated on the rotor surface. Under varied uniform wind velocities of 7, 8, 9, and 10 m/s, the effect of collective pitch control and cyclic pitch control on the power coefficient and thrust coefficient of FOWT is then discussed. Furthermore, at a wind speed of 10 m/s, both the power coefficient and loads are investigated as the pitch angle and yaw angle change. Experimental results indicate that the combined moment magnitude can be controlled by changing the pitch-angle amplitude. The power coefficient is adjusted by the cyclic pitch-angle controller when the pitch-angle phase changes. In addition, the thrust coefficient fluctuated when the pitch angle changed in the oblique inflow wind condition.

Keywords: floating offshore wind turbine; load reductions; collective pitch control; cyclic pitch control; wind tunnel experiment



Citation: Sang, L.Q.; Li, Q.; Maeda, T.; Kamada, Y.; Huu, D.N.; Tran, Q.T.; Sanseverino, E.R. Study Method of Pitch-Angle Control on Load and the Performance of a Floating Offshore Wind Turbine by Experiments. *Energies* **2023**, *16*, 2762. <https://doi.org/10.3390/en16062762>

Academic Editor: Davide Astolfi

Received: 30 January 2023

Revised: 2 March 2023

Accepted: 13 March 2023

Published: 16 March 2023



Copyright: © 2023 by the authors. Licensee MDPI, Basel, Switzerland. This article is an open access article distributed under the terms and conditions of the Creative Commons Attribution (CC BY) license (<https://creativecommons.org/licenses/by/4.0/>).

1. Introduction

The demand for using energy to develop economic, production, and other sectors in the world has been increasing at high speed in recent decades. Therefore, providing enough energy for growing the demand for energy consumption is a challenge for power generation development. Besides, renewable energy has many advantages such as the rapid decline in capital costs, air quality improvements, and reduction of carbon emissions [1]. Among renewable energies, wind energy is the one showing a continuous and accelerated growth.

For onshore wind power, the installed capacity has reached about 72.5 GW, and the offshore wind power installed capacity has gone beyond 21 GW [2]. Until recent times, offshore wind energy has been deployed near shore (at depths below 60 m) using the traditional fixed bottom substructures or conventional concrete gravity foundation. Additionally, floating technology is used for deep-water areas (from 60 m to 200 m), and it is a promising technology for the future because of technical improvements and possible larger scale developments. For these reasons, the investment costs of offshore wind power projects will reduce in the coming years [3].

Because the size of the offshore wind turbine (comprising tower, blade, generator) increases rapidly, dynamic loads of the blade and wind turbine are larger when the floating offshore wind turbine operates [4–6]. The fluctuations of these dynamic loads can be divided into three groups: the tower vibration, blades or rotor loads, and the variation of aerodynamic torque and output power. To limit the tower vibration, the pitch angle is increased. In this way, tower fore-aft fluctuations [7,8] are reduced. For blades or rotors, the individual blade pitch control is used to smooth the blade load fluctuation or reduce the main periodic load components [9,10]. Multivariable linear parameter-varying control techniques are applied to decrease the structural loads [11]. Additionally, a fuzzy-logic proportional control method is exhibited to decrease the moment load on the rotor and tower with fixed output power [12]. For the aerodynamic torque and output power control, a multivariable disturbance observer is introduced [13] to decrease the output power vibration, tower oscillation, and drive-train torsion. The individual pitch-control method reduces the 3P fluctuating component of the output power under different wind speed conditions [14]. Therefore, in the latter work, loads are mitigated as possible solution and suitable control methods have been selected.

For increasing the cost effectiveness of the floating offshore wind power projects, the capital cost of the wind turbine needs to be limited as it strongly affects the total investment capital. The structure of a 2-bladed wind turbine will reduce the cost of the material for less than one blade, while showing a quicker installation [15]. Hence, a 2-bladed wind turbine is considered for the experimental part of this research. In the past, this wind turbine technology was not fully considered because of its asymmetrical rotation, visual, and noise impact [16]. However, the effect of noise on the installation and operation phase of offshore wind turbines (pile-driving noise or vessel noise) was considered [17–19]. Moreover, the asymmetry issue is investigated. The loads are caused by the asymmetry, depending strongly on the azimuth angle. A teeter hinge and active mechanisms are used to reduce loads of the wind turbine [20–22]. As compared with 3-bladed upwind or downwind wind turbines, the 2-bladed downwind has higher power, large tip speed ratio, and a lighter rotor [23,24].

Researchers and authors have introduced controlled methods for increasing the power and reducing loads of wind turbines. For blades, methods can be divided into two types: modifying the blades, and eliminating the reforming ones. The first type, blade-modified methods, comprise the use of trailing edge flaps, micro tabs, and synthetic jet actuators [25,26]. On the other hand, still working on the blades without changing their structure is listed in what follows: collective pitch control, individual pitch control, pitch-to-stall, and pitch-to-feather [27,28]. The rotational torque is controlled by the collective pitch angle in full load conditions [29]. A PID controller gets the signal from the generator speed to control the collective pitch angle. Using this method, the collective pitch control cannot reduce the harmonic loads due to the asymmetric loads on the rotor plane [30]. In other studies, authors used light detection and ranging (LIDAR) technology to decrease the 1P frequency harmonic loads based on wind measurement. Simple collective pitch controllers can reduce loads of the wind turbine structures when receiving feedback signs from the LIDAR system [31,32]. An individual pitch control (IPC) is applied to reduce the load of the wind turbine. One advantage over commercial turbines is that the braking systems are independent, getting rid of a high-capacity shaft brake [33]. Therefore, the pitch angle of each blade can be controlled individually [34]. Specifically, the measured blade loads are

transformed to a single-input, single-output (SISO) controller; then, the control command is set up and the demand pitch angle is obtained [22,33].

FOWTs are mounted on platforms that must bear the complex dynamic load. Stochastic loads of the tower (and rotor blades) deriving from wind and waves are the main factors that need to be reduced for stabilizing the power production and load mitigation. The blade pitch controller of FOWTs is a key method under above-rated wind speeds. It can generate negative damping of the floating foundation [28,35–37]. The cyclic pitch-control method significantly reduces the teeter angle when operating in normal and extreme gust conditions [38]. The performance and aerodynamic forces are controlled by the cyclic pitch-control method in the diagonal inflow wind [39]. However, the wave forces are difficult to eliminate by the feedback control method [40,41]. In [42], a multi-input multi-output (MIMO) system estimates the importance of the control inputs generator torque and blade pitch angle for the rejection of wind and wave loads.

In this paper, the purpose of this work is to investigate the force under the collective pitch angle and cyclic pitch-angle control on the power coefficient, thrust coefficient, and the aerodynamic load of the 2-bladed downwind wind turbine. The pitch-angle control includes the collective pitch angle and the cyclic pitch-angle control. In these experiments, the wind speed variation and misalignment are taken into consideration. The results of this study can help researchers to better understand these control methods on the rotational rotor plane of the wind turbine.

The structure of the paper is organized in four sections: Section 1 presents the introduction. Section 2 shows the experimental types of equipment used, wind conditions, and calculation equations. Section 3 discusses the output experimental data, and the conclusion, Section 4, is reported at the end.

2. Experimental Conditions and Method

This section contains a detailed description of the experiment including an opened wind tunnel of the Mie University in Japan and key devices such as a 2-bladed downwind wind turbine, a pitch-angle control system, and Avistar blades. A brief description of the wind tunnel, the model wind turbine, a swash plate device, the overall setup, and measurement system are also given.

2.1. Experimental Method

2.1.1. Opened Wind Tunnel

Experiments for the pitch-angle control have been carried out in the opened wind tunnel. A sketch of the wind tunnel is reported in Figure 1.

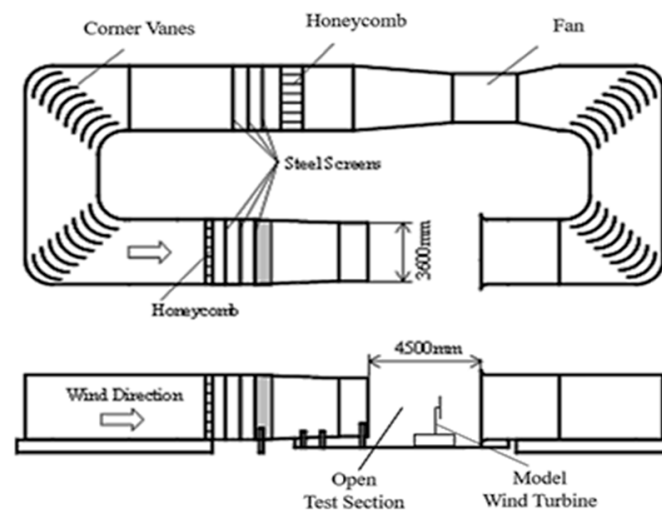


Figure 1. An overall diagram of the wind tunnel for the experiment.

The opened circular wind tunnel has an outlet diameter of 3.6 m, and the air collector size is 4.5 m × 4.5 m. A model of a 2-bladed downwind wind turbine is located in the Open Test Section. The wind turbine has blades with the length of 0.8 m.

The test section area, where the wind turbine is located, has a length of 4.5 m. The mainstream speed has maximum value of 30 m/s. Pitot tube installed at the wind tunnel outlet measures the mainstream wind speed.

The room temperature is measured by a platinum-resistance temperature detector. The experimental results are calculated based on the Cartesian coordinate with the x , y , and z -axes setting in the mainstream, the lateral, and the vertical directions.

Honeycombs installed in front of the outlet reduce the turbulence intensity. The speed deviation at the center line of the hub height is 1.5% or less, and the turbulence intensity is 0.50% or less. This data is measured by the laser Doppler and the heat ray velocimeter. Maeda et al. [43] and Li et al. [44] presented the effect of the blockage on the downwind wind turbine in previous studies.

2.1.2. The 2-Bladed Downwind Wind Turbine Model

The 2-bladed downwind wind turbine model used in this experiment is a horizontal axis-type and installed at the test section with a distance from the outlet of 3084 mm (from the rotor of the wind turbine to the outlet) (seen in Figure 2a).

The diameter of the rotor is $D = 1600$ mm, and the hub height is 1.535 m. The rotor speed is controlled by a variable speed generator installed in the nacelle. The rotor speed is controlled via the changeable speed-generator driver, and variable speed-generator amplifier, sending the command value from a personal computer as a digital value. The rotational speed of the generator is 880 rpm. The wind speeds in this experiment are 7, 8, 9, and 10 m/s. The blades are manufactured by Avistar airfoil. The chord length and twist angle of the blade are reported in Figure 2b.

In order to consider the stability of the Avistar blade, experiments affected by the low Reynolds numbers of $Re = 0.5 \times 10^5$, 1.0×10^5 , 1.5×10^5 , and 2.0×10^5 on the airfoil performance were carried out and there is no significant effect on the aerodynamic performance of the blades [45]. Therefore, the data of the experiment is correct and reliable.

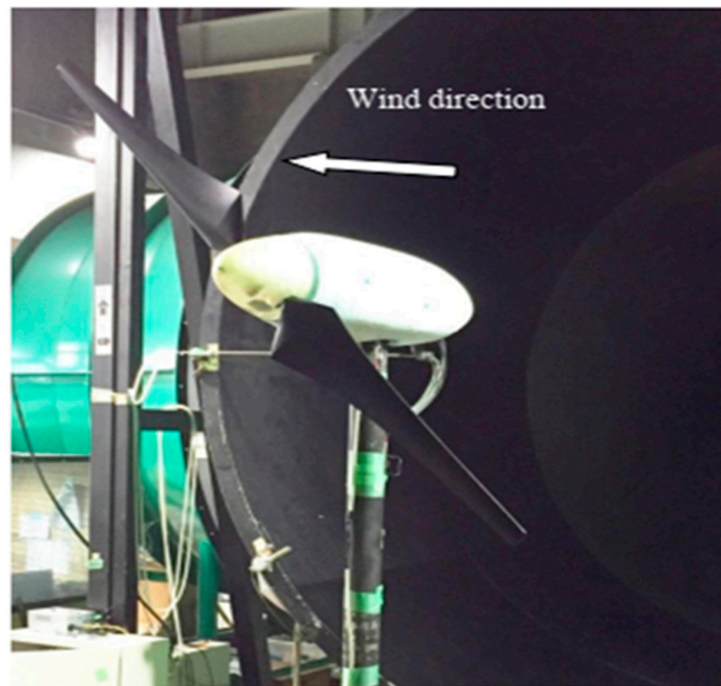
A six-component balance device is set up between the nacelle and the tower of the wind turbine model. The forces and moments are measured by this device following the three directions of x , y , and z -axes. The digital measurement values are collected and treated by the personal computer. In addition, the load measuring point location in this experiment is the center of the rotor; it is the origin coordinate in the measurement.

2.1.3. Pitch-Angle Control Device

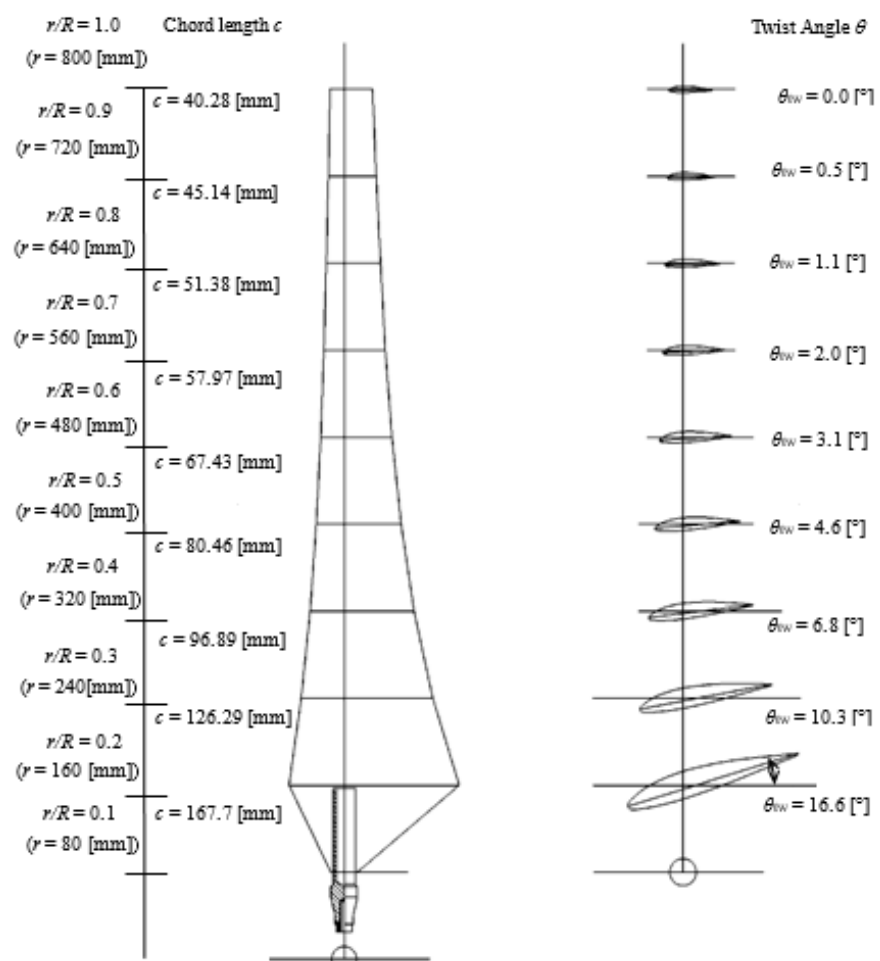
Actuators installed inside the nacelle control the pitch angle of the blade of the wind turbine. These actuators are linear drive actuators that incorporate a ball screw into stepping motors with built-in rotor position sensors. The pitch angle of the blade is changed when the operator sets up commands from a personal computer to control the actuator driver. Besides, a swash plate adjusts the pitch angle following the azimuth angle as exhibited in Figure 3a. This equipment is organized by a non-rotating disc, a rotating disc, and a bearing. Three actuators are installed at three positions with the azimuth angles of $\psi = 0^\circ$, 120° , and 240° as exhibited in Figure 3b.

The swashplate includes a non-rotating part and a rotating part. The swashplate can adjust the collective pitch angle and the cyclic pitch angle.

For this experiment, both the collective pitch and the cyclic pitch angle are changed to estimate the phenomena of the power coefficient. The swashplate moving parallel with the rotor surface will make the collective pitch angle. Further, the cyclic pitch control followed by the azimuth angle is performed when the swashplate moves title with the rotor surface. The angle between the chord line and the rotor's plane is called the pitch angle. The yaw angle is the angle between the wind direction and the wind turbine axis.

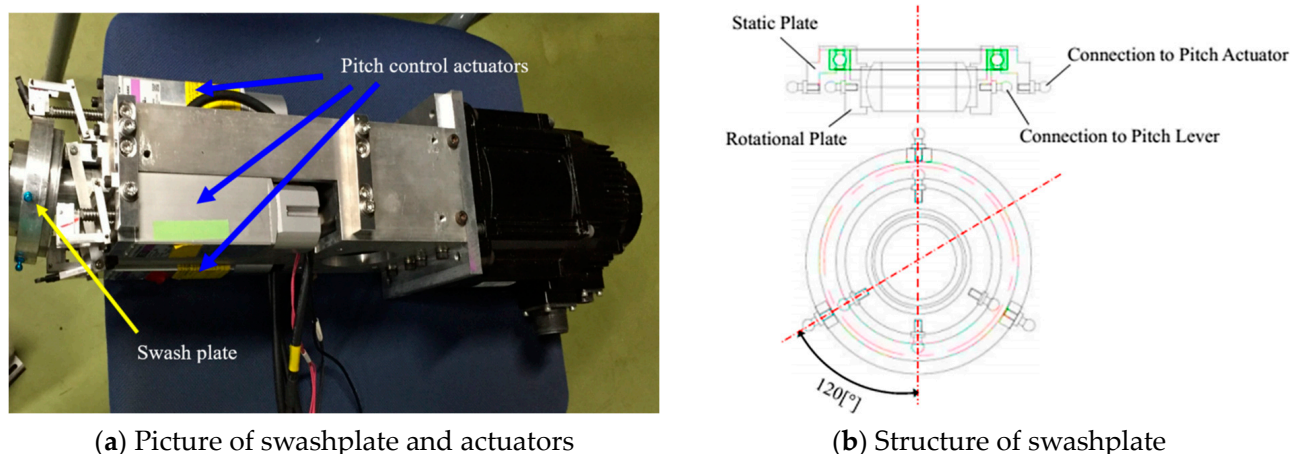


(a) The 2-bladed downwind wind turbine model



(b) Detailed view of Avistar blade

Figure 2. Wind turbine model and Avistar blade.



(a) Picture of swashplate and actuators

(b) Structure of swashplate

Figure 3. Swashplate equipment for controlling the pitch angle.

2.2. Input Data for the Experiment

Two pitch-angle control methods are used to estimate the change of the power and thrust coefficient in the steady and diagonal inflow wind conditions. Besides, the effect of the change of the pitch angle and yaw angle on the power coefficient and moments on the wind turbine are also investigated. The power and thrust coefficient are considered with the mainstream wind velocity of 7, 8, 9, and 10 m/s. In the collective pitch-control experiment, the power and thrust coefficient are considered in the conditions of the pitch angle of $\theta = -1, 0, +1$ [°], the mainstream speed of $U = 10$ [m/s], and the maximum tip speed ratio of $\lambda = 7.4$. The load of the wind turbine is estimated based on the pitch moment and yaw moment. In another experiment, the cyclic pitch-angle control is studied in the diagonal wind condition, with the yaw angles of $\varphi = -5, 0, +5$ [°]. The experimental conditions are summarized in Table 1.

Table 1. Input data of the experiment.

Wind Velocity [m/s]	Pitch Angle θ [°]	Pitch-Angle Amplitude [°]	Pitch-Angle Phase [°]	Yaw Angle [°]
7, 8, 9, 10	$-1^\circ, 0^\circ$ and 1°	$a = -1^\circ \sim 1^\circ$	$\zeta = 0^\circ, 45^\circ, 90^\circ, 135^\circ$ and $\zeta = 30^\circ, 60^\circ, 120^\circ, 150^\circ$	$-5^\circ, 0^\circ, 5^\circ$

The angle created by the chord line and the relative wind direction is called the angle of attack. The angle of attack changes over the entire rotor surface due to the twist angle. The fluid force on the blades is also expected to change. Therefore, the fluid force appearing on the rotor surface can change. The pitch angle is constant at all azimuth angle positions during the experimental process.

2.3. Calculation Formulas

The pitch angle is calculated as follows:

$$\theta(\psi) = a \cos(\psi - \zeta) + b \quad (1)$$

Here, ψ is the azimuth angle; ζ is the phase angle of the pitch angle θ with respect to the azimuth angle ψ ; a is the pitch-angle amplitude; and b is the average pitch angle.

The power coefficient, thrust coefficient, and the tip speed ratio are calculated as follows:

$$\lambda = \frac{R\omega}{U} \quad (2)$$

$$C_P = \frac{P}{0.5\rho AU^3} \quad (3)$$

$$C_T = \frac{T}{0.5\rho AU^2} \quad (4)$$

Regarding Equations (2)–(4), P and T denote the rotor performance and the rotor thrust force; R represents the rotor radius [m]; ρ the density of air [kg/m^3]; A is the swept area of the rotor [m^2]; U is mainstream wind speed [m/s]; and ω is the angular velocity [rad/s].

The pitching moment coefficient, C_{Mx} , and the yaw moment coefficient, C_{Mz} , are calculated:

$$C_{Mx} = \frac{Mx}{0.5\rho U^2 AR} \quad (5)$$

$$C_{Mz} = \frac{Mz}{0.5\rho U^2 AR} \quad (6)$$

Here, Mx is the pitching moment, and Mz is the yaw moment.

When the pitch angle changes, the angle of attack also changes on all the rotor's span. Therefore, the fluid force acting on the blades also changes.

The angle of attack at each airfoil can be obtained through the following equation:

$$\alpha = \phi - (\beta + \theta_{\text{twist}}) \quad (7)$$

Calculate the angle of attack as follows [46]:

$$\alpha = \tan^{-1} \left[\frac{(1-a)U_0}{(1+a')\Omega r} \right] - (\theta_{\text{twist}} + \beta) \quad (8)$$

3. Results and Discussion

The stability of the offshore wind turbine is an important issue when it operates on the sea. However, more improvement is required to expand the installation in deep water offshore areas. Therefore, in this study, the flow force acting on the rotor's area of the wind turbine was focused on, and the experiment was conducted by trying to suppress the shaking of the floating offshore wind turbine. The aerodynamic characteristics of the wind turbine are described under the front inflow wind and oblique wind conditions. The experiment to deduce the wind turbine performance is conducted to acquire basic data about the wind turbine. The pitch-angle control experiment is also carried out to measure the fluid force on the rotor's area when the pitch angle is adjusted.

The pitch-angle control experiment includes the collective pitch-control test that keeps the pitch angle constant concerning the azimuth angle. Besides, the cyclic pitch-control test adjusts the pitch angle followed the azimuth angle according to Equation (1). The flow force on the blade element is indicated in Figure 4.

In the figure, the flow force impacting the blade element surface increases since the lift force rises and the drag force degrades. The inflow angle acting on the low wind speed region is large. When the angle of attack obtains the optimum value, the power coefficient is also at a high level. The inflow angle acting on the high wind speed region is small, the pitch angle is small, and the angle of attack is sufficiently large to generate the lift force.

3.1. Collective Pitch Control

The wind turbine model was tested in the wind tunnel to consider the power coefficient curves in the wind speed conditions of 7, 8, 9, and 10 m/s as exhibited in Figure 5. The horizontal axis indicates the tip speed ratio λ , and the vertical axis presents the output power coefficient C_P .

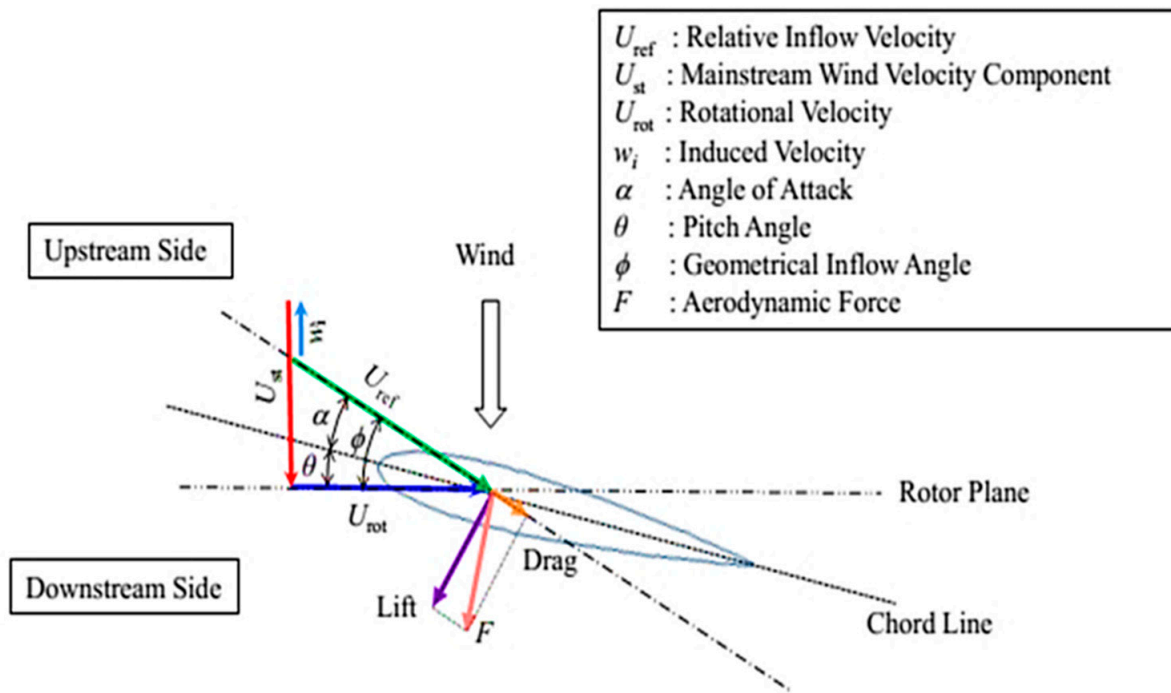


Figure 4. Flow force on blade element with the positive pitch angle.

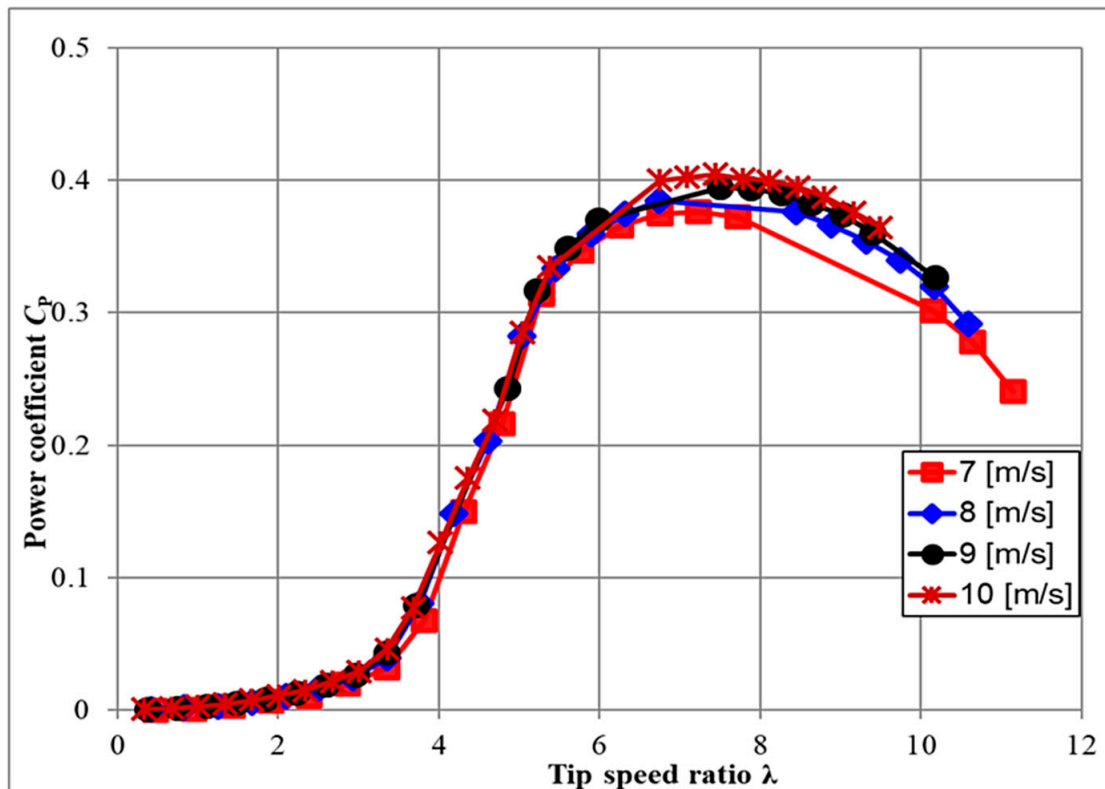


Figure 5. The power coefficient changes under different wind speeds 7, 8, 9 and 10 m/s.

From the figure, at any wind speed, the output power coefficient C_p increases as the tip speed ratio λ increases to reach the maximum value and then decreases. The angle of attack increases in the low tip speed ratio region. As a result, the blade has an excessive angle of attack, the lift force decreases, the drag force increases, and the power coefficient

goes down. When the angle of attack becomes smaller in the high tip speed ratio region, the peak power coefficients are $C_P = 0.3943, 0.3947, 0.403,$ and 0.408 at $\lambda = 7.22, 6.74, 7.5,$ and 7.43 at the mainstream wind speed conditions of $U = 7, 8, 9,$ and 10 m/s, respectively. From experimental results, the optimum power coefficient obtains $C_P = 0.408$ as the tip speed ratio of $\lambda = 7.43$ and the wind speed of $U = 10$ m/s. This issue indicates that the maximum power coefficient increases due to raising mainstream wind speed. It is considered that the relative blade inflows increase as the mainstream wind speed increases and the Reynolds number on the blade element goes up.

Similarly, the thrust coefficient curves were also experimented in the wind speed of 7, 8, 9, and 10 m/s as presented in Figure 6.

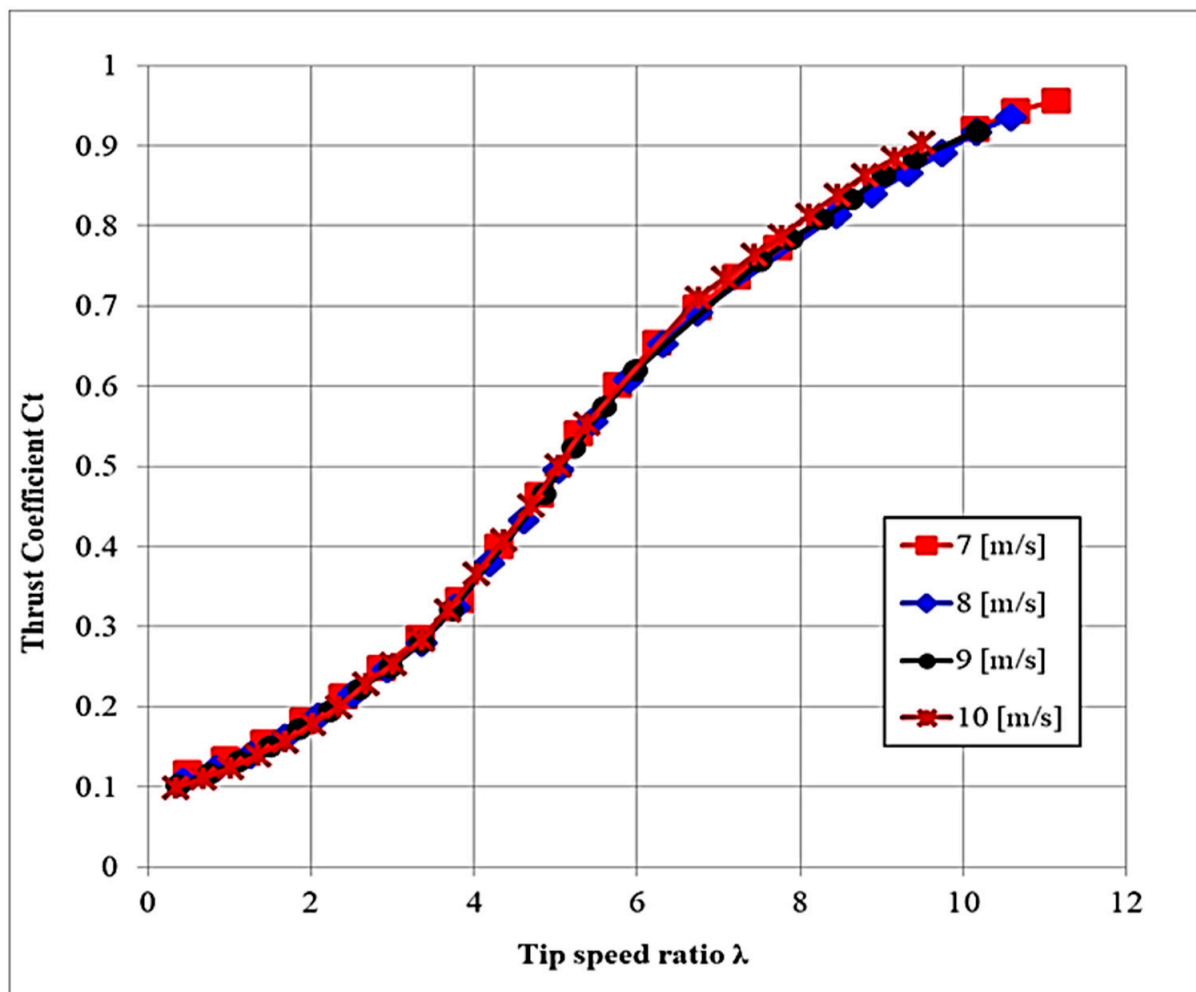


Figure 6. The thrust coefficient changes under different wind speeds 7, 8, 9 and 10 m/s.

The thrust coefficient C_T increases monotonically when the tip speed ratio λ increases at any wind speed as exhibited in Figure 6. The thrust coefficient value is $C_T = 0.76$ at the optimum tip speed ratio of $\lambda = 7.43$ and the wind speed of $U = 10$ m/s. There is almost no difference in the thrust coefficient with the different wind speeds. The thrust force is generated by the lift force on the blade elements of the rotor blades. The lift coefficient depends on the angle of attack of the blade element. Therefore, the angle of attack is similar at the same tip speed ratio, and it does not depend on the mainstream wind speed. In addition, the Avistar airfoil used for this experiment did not depend on the low Reynolds number. The Reynolds number in the wind tunnel is within the range presented in Section 2.1.2.

The relationship between the thrust and the power coefficient is also considered in the next study. The thrust force can be adjusted during the collective pitch-control process, but at the same time, the power also changes secondarily. The horizontal axis indicates the power and the thrust coefficient, and the vertical axis is the amplitude of the power and the thrust coefficient. The optimum values of the power and the thrust coefficient are different when the pitch angle changes as indicated in Figure 7.

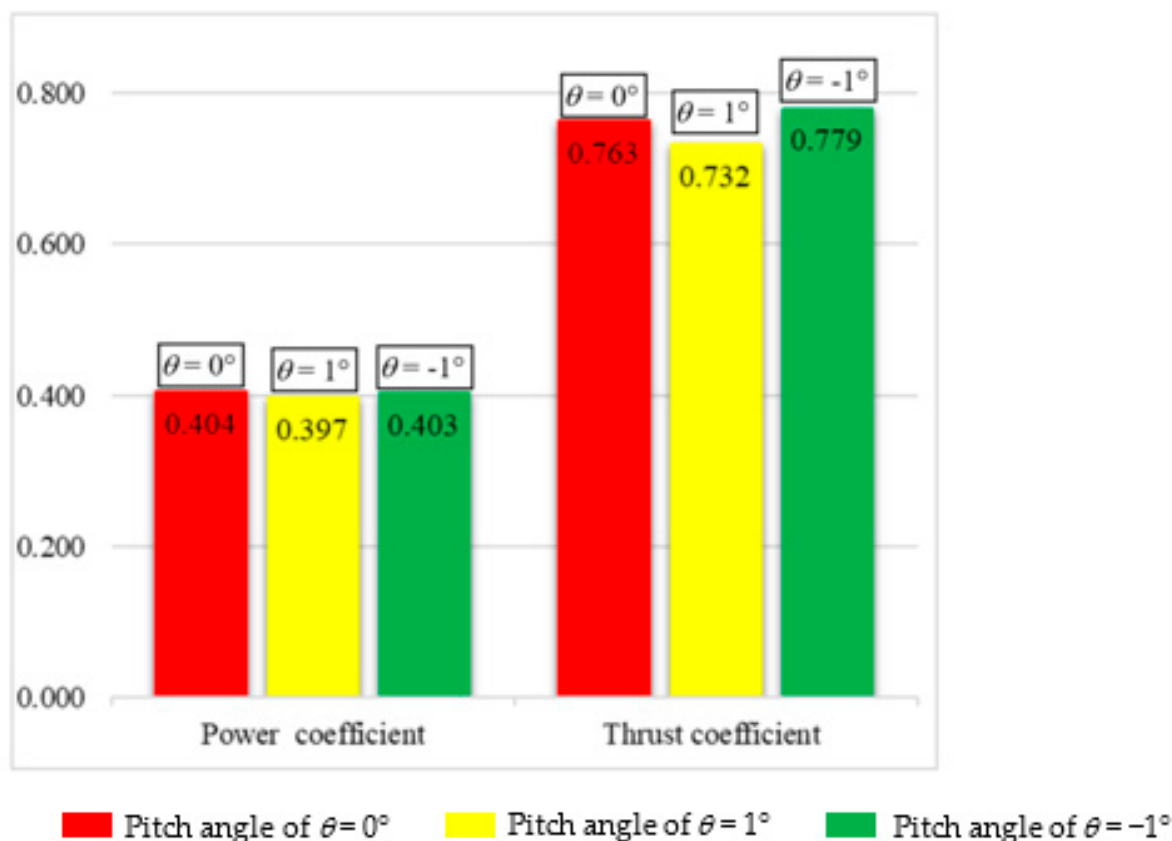


Figure 7. The optimum values of the power and the thrust coefficient are different when the pitch angle changes with $\theta = -1^\circ, 1^\circ$, and 0° at the yaw angle of $\varphi = 0^\circ$.

The pitch angles corresponding to the plot in Figure 7 show changes of 1 degree for the different colored bars.

The lowest thrust coefficient is $C_T = 0.732$ at the pitch angle of $\theta = 1^\circ$, while it increases for a pitch-angle reduction (-1°). From the figure, the power coefficient C_P becomes maximum when the thrust coefficient is $C_T = 0.763$ at the pitch angle $\theta = 0^\circ$ and decreases in both cases of going up and going down from the optimum pitch angle. Therefore, when controlling the thrust force by the pitch angle, the power decrease can be limited by setting the pitch angle smaller than the optimum pitch angle.

Similarly, the thrust and the power coefficient are also investigated in the oblique inflow wind of $\varphi = -5^\circ, 0^\circ, 5^\circ$ when the pitch angle changes. Figure 8 exhibits the relationship between the power and the thrust coefficient in the oblique inflow wind condition.

The pitch angle changes from -1° to 1° at 0.5° intervals. The yaw angles of $\varphi = -5^\circ, 0^\circ, 5^\circ$ are green, red, and yellow color lines, respectively. At the yaw angle declination, the thrust coefficient of $C_T = 0.715$ is the lowest at $\varphi = 5^\circ$ and $\theta = 1^\circ$, and it is increasing in the direction of the pitch-angle reduction. From the figure, the power coefficients C_P at the yaw angles of $\varphi = 0, \pm 5^\circ$ decrease in both cases of going up and going down from the maximum point of the power coefficient. The power coefficient and the thrust coefficient fluctuate in the oblique inflow wind. Therefore, the thrust force is adjusted by

the pitch-angle change in the oblique inflow wind by setting the pitch angle smaller than the optimum pitch-angle value.

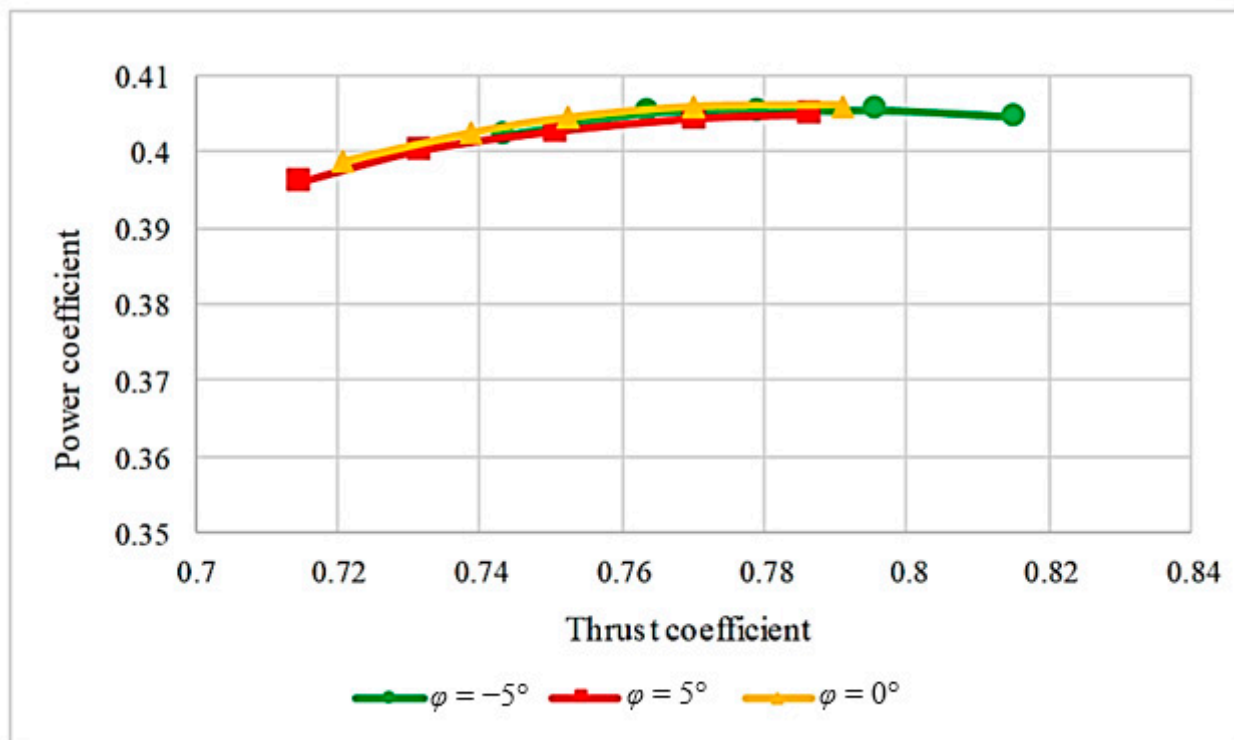


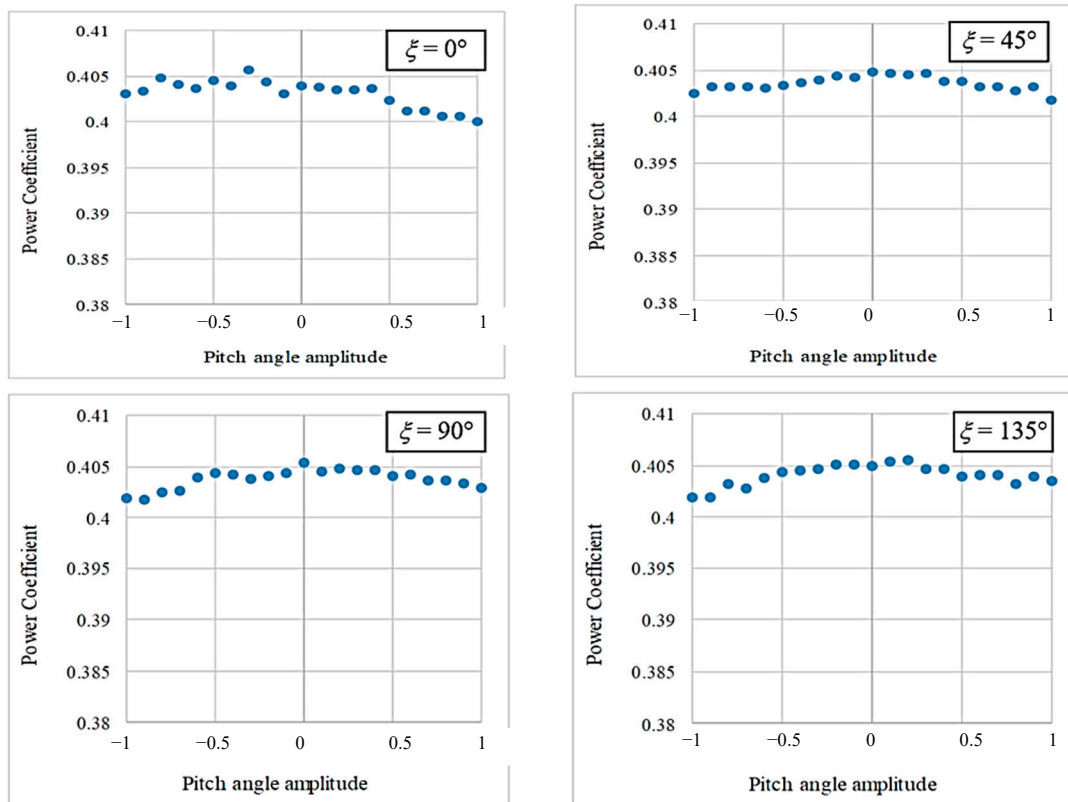
Figure 8. Relationship between the power and thrust coefficient when the change of the yaw angle is $\varphi = -5^\circ, 5^\circ$ and 0° at $\theta = 0^\circ$.

3.2. Cyclic Pitch Control

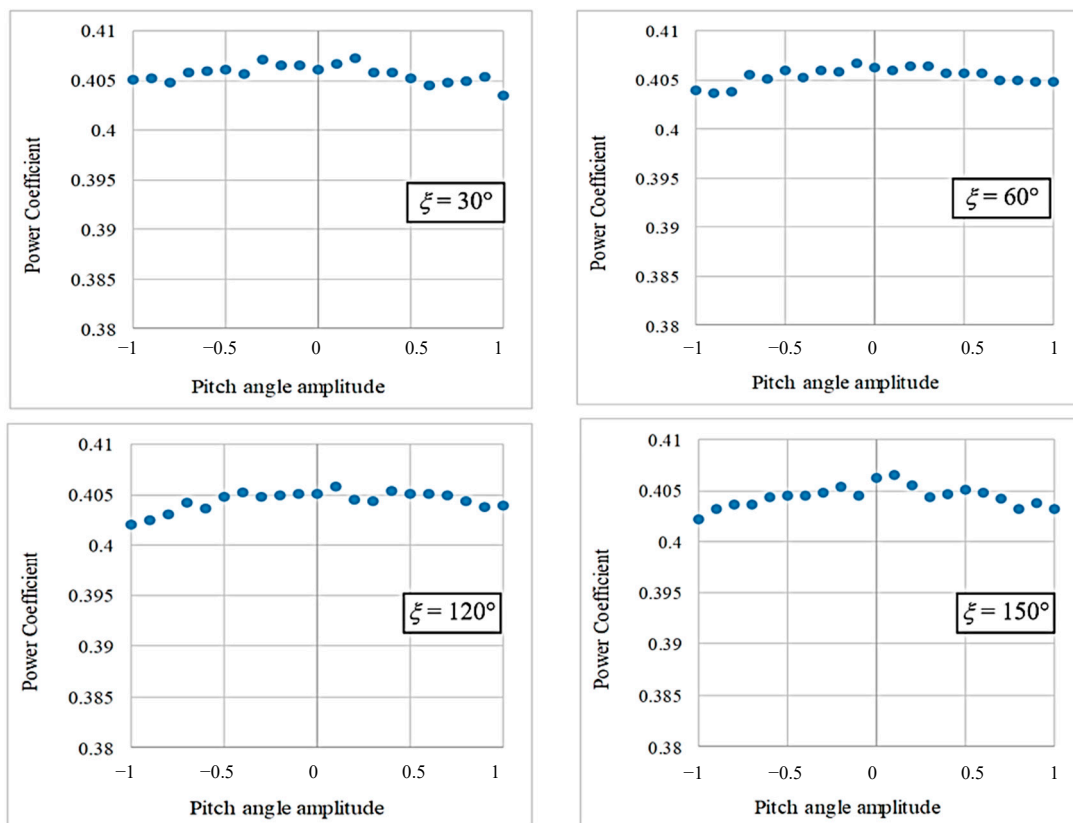
In this section, the experimental data are analyzed to understand the effect of this control method on the power coefficient and load. The pitch-angle amplitude changes from -1° to 1° at 0.1 intervals. The phase angle is divided into two cases of $\zeta = 0^\circ, 45^\circ, 90^\circ$, and 135° , and the $\zeta = 30^\circ, 60^\circ, 120^\circ$, and 150° .

Figure 9a,b describe the effect of the pitch-angle amplitude change on the power coefficient with the phase angle defined as above at the averaged pitch angle $b = 0^\circ$.

For the cyclic pitch control as Equation (1), the pitch angle of the blade is calculated by a cosine function. When the rotor turns repeatedly in a rotation from 0° to 360° , it leads to the azimuth angle of the pitch angle fluctuating according to the azimuth angle rotation. The power coefficient at the phase angle of $\zeta = 0^\circ$ has stronger fluctuation than others as exhibited in Figure 9. This can be seen as the angle phase changes, and the power coefficient oscillates following the pitch-angle amplitude. Therefore, the power coefficient of the wind turbine can be affected by the azimuth angle rotation. In addition, the maximum power coefficient depends on the azimuth angle rotation in the pitch-angle amplitude range from -1° to 1° ; this happened due to the azimuth angle rotation. The value of the maximum and minimum of the pitch angles depends on each phase angle. The fluctuation of the power coefficient at the pitch angle differing from 0° is smoother than the phase angle of $\zeta = 0^\circ$. Therefore, it is controlled by the cyclic pitch control when the azimuth angle rotates.



(a)



(b)

Figure 9. Depiction of the effect of the cyclic pitch control on the power coefficient. The phase angle is divided into two cases of (a) $\xi = 0^\circ, 45^\circ, 90^\circ$, and 135° , and (b) $\xi = 30^\circ, 60^\circ, 120^\circ$, and 150° .

3.3. Moments on the FOWT

In this study, the slope of the moments (pitching and yaw moment) is called the moment axis angle ψ_M , and the equation for deriving ψ_M from $C_{Mx}(\zeta, a)$, $C_{Mz}(\zeta, a)$ is shown in the following equation:

$$\psi_M(\zeta, a) = \tan^{-1} \left[\frac{-C_{Mx}(\zeta, a)}{C_{Mz}(\zeta, a)} \right] \tag{9}$$

where $C_{Mx}(\zeta, a)$ and $C_{Mz}(\zeta, a)$ are the results of subtraction of the pitching moment and the yaw moment at the pitch-angle amplitude of a for $a = 0^\circ$.

Consider the relationship between the moment-axis azimuth and the pitch-angle amplitude as indicated in Figure 10. The fluctuation of the moment-axis angle $\psi_M(\zeta, a)$ when the pitch-angle amplitude a changes during the periodic pitch-angle control with the phase angle of $\zeta = 0^\circ, 45^\circ, 90^\circ,$ and 135° , and the $\zeta = 30^\circ, 60^\circ, 120^\circ,$ and 150° .

The pitch-angle amplitude of $a = 0 [^\circ]$ is the reference point and has no slope, so the plot is omitted. The moment-axis angle is almost constant in the same phases ζ , and unaffected by the change of the change amplitude a . Figure 11 exhibits the correlation between the phase angle ζ and the moment-axis angle $\psi_M(\zeta)'$ and the approximate curve.

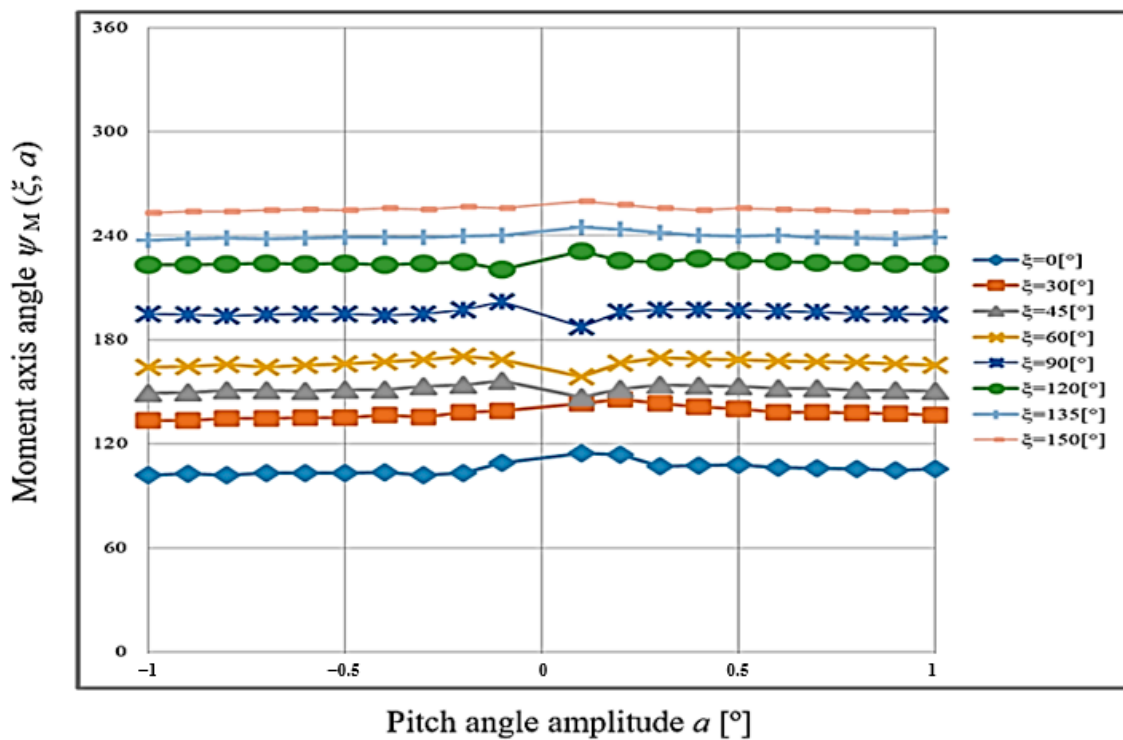


Figure 10. Relationship between the moment-axis azimuth and the pitch-angle amplitude with the phase angle of $\zeta = 0^\circ, 45^\circ, 90^\circ,$ and 135° , and $\zeta = 30^\circ, 60^\circ, 120^\circ,$ and 150° .

The horizontal axis of the figure is the pitch-angle phase ζ and the vertical axis presents the moment-axis angle $\psi_M(\zeta)'$. The moment-axis angle $\psi_M(\zeta)'$ fluctuates linearly with the phase angle ζ as indicated in Figure 11. Besides, there is a difference in $\psi_M(\zeta)'$ concerning the pitch-angle phase ζ . It means that the azimuth angle, which indicates the difference between the flap moments on the rotor, lags behind the azimuth angle, which shows the maximum pitch-angle amplitude. The phase difference of $\psi_M(\zeta)'$ with respect to this phase ζ is defined as ψ_{dis} . The approximate straight line in Figure 11 is shown in the following E = Equation (10).

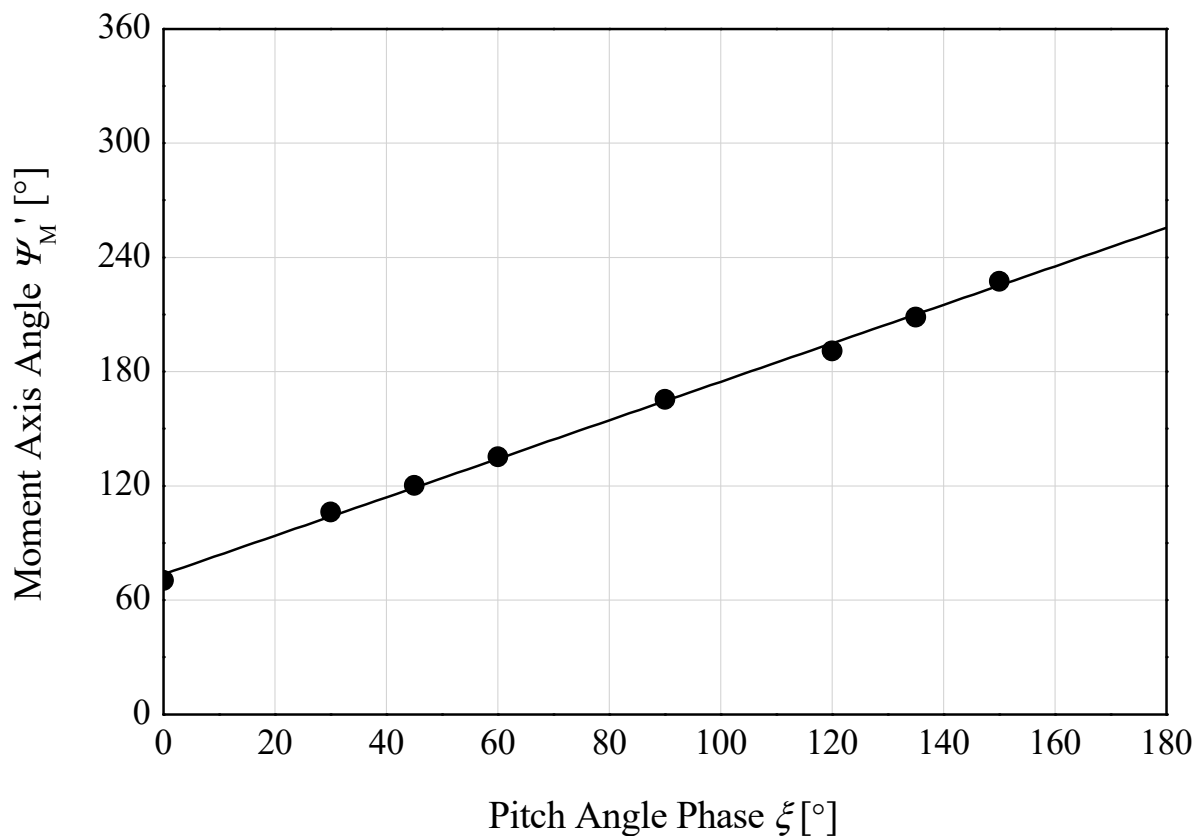


Figure 11. Relationship between the moment-axis angle and the angle phase.

$$\psi_M(\xi)' = 1.01\xi + 73.5^\circ \quad (10)$$

From Equation (8), the y-intercept is $\psi_{\text{dis}} = 73.5$ [°]. This phase difference ψ_{dis} is due to the changes in the moment on the rotor area because the angle of attack of the blade element fluctuates due to the oblique inflow wind and the lift generated changes. Next, the magnitude of the moment acting around the axis is combined and factorized into $C_M(\xi, a)$. The calculation formula of $C_M(\xi, a)$ is shown in the following:

$$C_M(\xi, a) = \sqrt{C_{Mx}(\xi, a)^2 + C_{Mz}(\xi, a)^2} \quad (11)$$

$$C_{M\text{mean}}(\xi) = \left(\sum_{a=-1.0}^{1.0} C_M(\xi, a) \right) \div 6 \quad (12)$$

Figure 12 shows the correlation between the change of the pitch-angle amplitude a at the phase angles of $\xi = 0, 30, 45, 60, 90, 120, 135,$ and 150 [°], and the combined moment coefficient $C_M(\xi, a)$.

The combined moment largely relates to the change pitch-angle amplitude of $a = -1$ to 1 [°], and it is almost unaffected by the phase angle. The combined moment coefficient $C_M(\xi, a)$ differs slightly because of the phase angle when the inflow velocity in the rotating surface is irregular. This effect happened due to the wake influence of the tower on the rotor area, and the wind blowing in the rotor changes at the different azimuth angles. Here, the average value of $C_M(\xi, a)$ in phase ξ of a certain change amplitude a is calculated and used as $C_{M\text{mean}}(\xi)$. The averaging equation is shown in the following Equation (13).

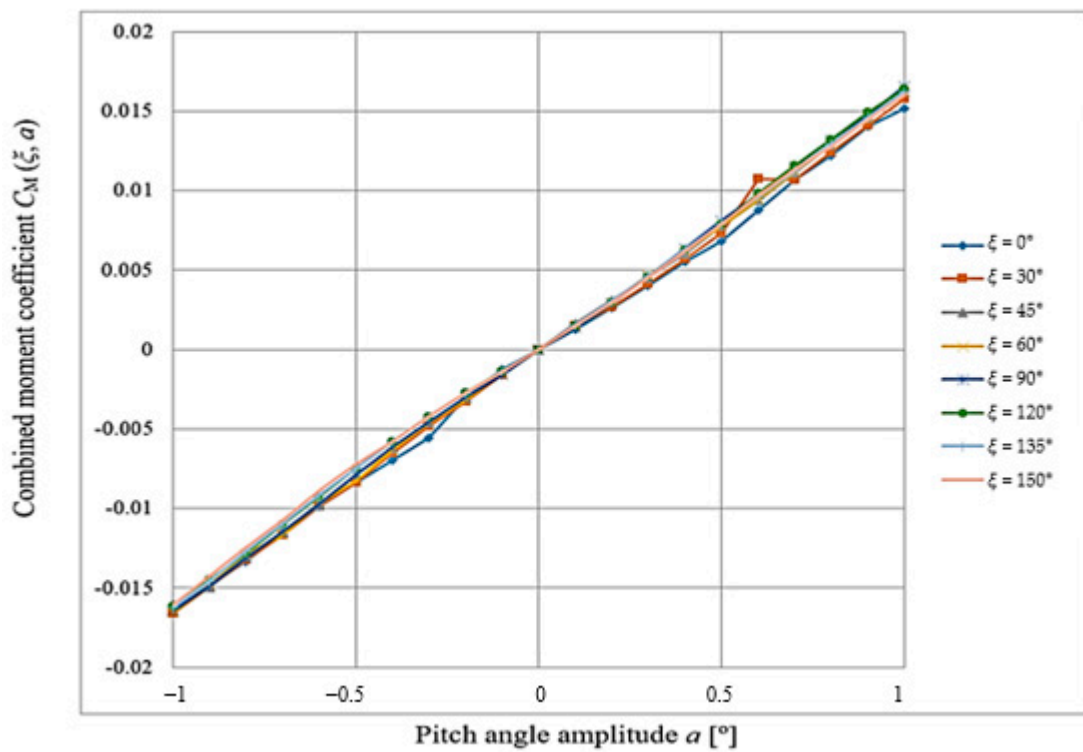


Figure 12. Relation between the combined moment and the pitch-angle amplitude with the angle phase of $\xi = 0^\circ, 30^\circ, 45^\circ, 60^\circ, 90^\circ, 120^\circ, 135^\circ$, and 150° .

Figure 13 indicates the relationship between the pitch-angle amplitude change and the average moment value $C_{Mmean}(\xi)$ of the combined moment coefficient $C_M(\xi, a)$.

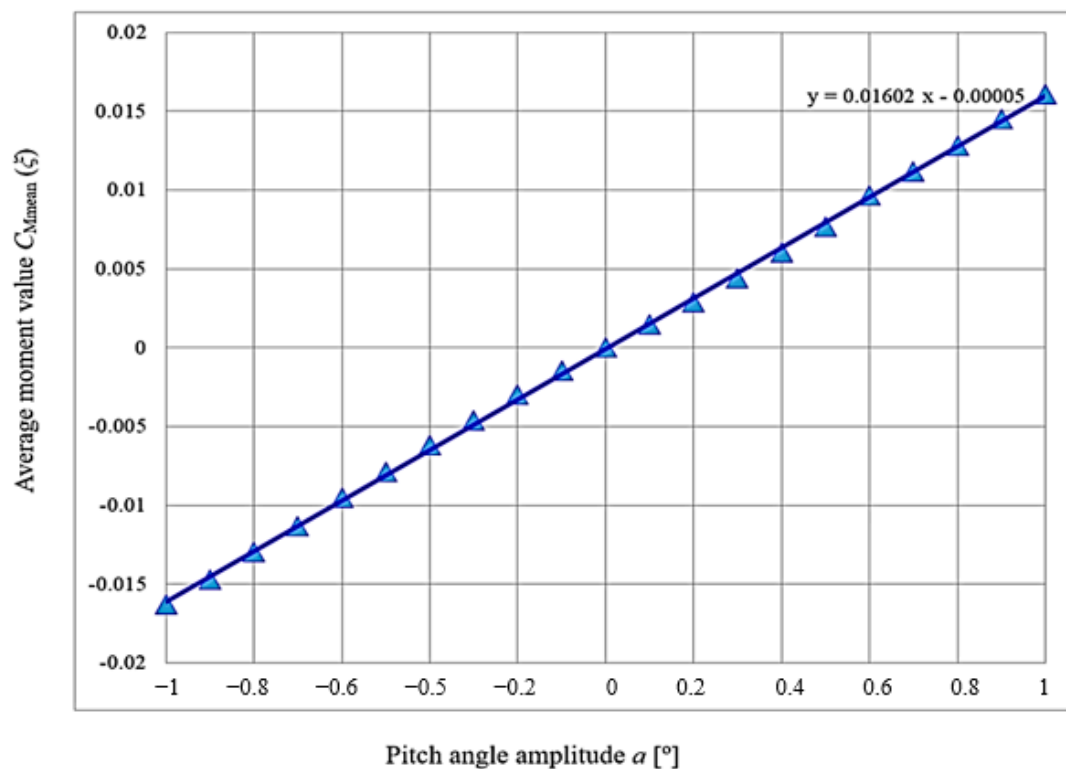


Figure 13. Correlation between the mean moment coefficient and the pitch-angle amplitude.

The horizontal axis shows the pitch-angle amplitude change a , and the vertical axis presents the average value $C_{Mmean}(\xi)$. From the figure, the average value $C_{Mmean}(\xi)$ changes linearly with the pitch-angle change amplitude. The combined moment coefficients $C_M(\xi, a)$ have a small difference in Figure 13. It can be considered the influence of the angle phase of the blade on the moments. In addition, the average value $C_{Mmean}(\xi)$ increases or decreases at a constant rate with respect to the pitch-angle amplitude change. The approximate straight line in Figure 13 is shown in Equation (13) below:

$$C_{Mmean}(\xi) = 0.01602x - 0.00005 \quad (13)$$

From Equation (13), with the pitch-angle amplitude a altered by 1° , the slope of the mean value $C_{Mmean}(\xi)$ of the combined moment increases or decreases by 0.01602. From this, the combined moment changes at a constant rate. Therefore, the combined moment can be controlled by adjusting the pitch angle.

From the above results, the pitch-control method can be proved for controlling the aerodynamic load effect on the rotor area during the rotating rotor process.

4. Conclusions

In this paper, the power and thrust coefficient of FOWT were estimated under the collective pitch angle and the cyclic pitch-angle control at different wind speeds of 7, 8, 9, and 10 m/s. This experiment tested the change of the power and thrust coefficient of the two-bladed downwind wind turbine in the wind tunnel. The swashplate was installed to control the pitch angle. In addition, the moments of the wind turbine model were also analyzed when the amplitude and phase angle of the pitch angle change. Following are the study's key findings in brief:

The wind speed significantly impacts the power coefficient. The optimum power coefficient was $C_p = 0.403$ at the tip speed ratio of $\lambda = 7.43$ and the wind speed of $U = 10$ m/s. Contrarily, there is almost no difference in the thrust coefficient for the different wind speeds under the uniform wind speed.

The thrust force is generated by the lift force acting on the blade elements, and the lift coefficient depends on the angle of attack of the blade element. Therefore, the thrust coefficient is adjusted by the pitch angle when the pitch angle and yaw angle changed.

The optimum power coefficient depends on the phase angle in the pitch-angle amplitude. The azimuth angle positions cause to change of the phase angle, leading to fluctuating power coefficients. Hence, the power coefficient is adjusted by the cyclic pitch-angle control method.

The moment-axis azimuth is almost constant in the same phases ξ in the pitch amplitude range from -1° to 1° . The magnitude of the combined moment largely depends on the change of the pitch-angle amplitude of $a = -1^\circ$ to 1° . And it is almost unaffected by the phase angle. Furthermore, the mean value $C_{Mmean}(\xi)$ of the combined moment increases or decreases by 0.01602. The pitch-control method can be proved for controlling the aerodynamic load effect on the rotor surface.

Author Contributions: Conceptualization, L.Q.S., Q.L., T.M., Y.K., D.N.H. and Q.T.T.; methodology, L.Q.S., Q.L., T.M. and Y.K.; validation, L.Q.S., Q.L., T.M. and Y.K.; writing—original draft preparation, L.Q.S., Q.L., T.M., Y.K. and Q.T.T.; writing—review and editing, L.Q.S., Q.L., T.M., Y.K., D.N.H., Q.T.T. and E.R.S. All authors have read and agreed to the published version of the manuscript.

Funding: This research received no external funding.

Data Availability Statement: The analytical and experimental data have been synthesized and presented in this paper.

Acknowledgments: Thank so much for the anonymous reviewers are acknowledged for their kind help and advice which have served to strengthen and clarify the paper. All individuals included in this section have consented to the acknowledgment.

Conflicts of Interest: The authors declare no conflict of interest.

References

1. IRENA. *Global Energy Transformation: A Roadmap to 2050*, 2019th ed.; International Renewable Energy Agency: Abu Dhabi, United Arab Emirates, 2019.
2. GWEC | Global Wind Report 2022; 158p. Available online: <https://gwec.net/global-wind-report-2022/> (accessed on 2 December 2022).
3. K&L Gates and SNC-Lavalin/Atkins. Offshore Wind handbook. Version 2. 2019. Available online: https://files.klgates.com/files/uploads/documents/2019_offshore_wind_handbook.pdf (accessed on 5 December 2022).
4. Haliade-X Offshore Wind Turbine. Available online: <https://www.ge.com/renewableenergy/wind-energy/offshore-wind/haliade-x-offshore-turbine> (accessed on 20 December 2022).
5. Siemens Gamesa Launches 14MW Offshore Wind Turbine, World's Largest. Available online: <https://www.greentechmedia.com/articles/read/siemens-gamesa-takes-worlds-largest-turbine-title> (accessed on 2 January 2020).
6. MHI Vestas Offshore Wind. World's Most Powerful Wind Turbine Once Again Smashes 24 hours Power Generation Record as 9 MW Wind Turbine is Launched. Available online: <http://www.mhivestasoffshore.com/new-24-hour-record/> (accessed on 2 January 2020).
7. Qiao, Y.; Han, S.; Deng, Y.; Liu, Y.; Dong, J.; Pan, L.; Li, R.; Zhao, B. Research on variable pitch control strategy of wind turbine for tower vibration reduction. *J. Eng.* **2017**, *2017*, 2005–2008. [[CrossRef](#)]
8. Lio, W.H.; Jones, B.L.; Rossiter, J.A. Estimation and control of wind turbine tower vibrations based on individual blade-pitch strategies. *IEEE Trans. Control. Syst. Technol.* **2019**, *27*, 1820–1828. [[CrossRef](#)]
9. Kanev, S.; Van, E.T. Exploring the limits in individual pitch control. In Proceedings of the European Wind Energy Conference and Exhibition, Marseille, France, 16–19 March 2009; pp. 679–704.
10. Coral-Enriquez, H.; Cortes-Romero, J.; Dorado-Rojas, S.A. Rejection of varying-frequency periodic load disturbances in wind-turbines through active disturbance rejection-based control. *Renew. Energy* **2019**, *141*, 217–235. [[CrossRef](#)]
11. Ossmann, D.; Theis, J.; Seiler, P. Load reduction on a clipper liberty wind turbine with linear parameter-varying individual blade pitch control. *Wind Energy* **2017**, *20*, 1771–1786. [[CrossRef](#)]
12. Civelek, Z.; Luy, M.; Cam, E.; Mamur, H. A new fuzzy logic proportional controller approach applied to individual pitch angle for wind turbine load mitigation. *Renew. Energy* **2017**, *111*, 708–717. [[CrossRef](#)]
13. Imran, R.M.; Hussain, D.M.A.; Chowdhry, B.S. Parameterized disturbance observer based controller to reduce cyclic loads of wind turbine. *Energies* **2018**, *11*, 1296. [[CrossRef](#)]
14. Zhang, Y.Q.; Hu, W.H.; Chen, Z.; Cheng, M. Individual pitch control for mitigation of power fluctuation of variable speed wind turbines. In Proceedings of the 10th International Power and Energy Conference (IPEC), Ho Chi Minh City, Vietnam, 12–14 December 2012; pp. 638–643.
15. 2-B Energy. Available online: <http://2benergy.com> (accessed on 20 December 2022).
16. Manwell, J.F.; McGowan, J.G.; Rogers, A.L. *Wind Energy Explained*; John Wiley & Sons: Chichester, UK, 2002.
17. Everley, K.A.; Radford, A.N.; Simpson, S.D. Pile-driving noise impairs antipredator behavior of the european sea bass *Dicentrarchus labrax*. In *The Effects of Noise on Aquatic Life II*; Springer: New York, NY, USA, 2016; pp. 273–279.
18. Farina, A.; Gage, S.H. *Ecoacoustics: The Ecological Role of Sounds*; John Wiley & Sons: Hoboken, NJ, USA, 2017.
19. Reyff, J. Underwater sounds from unattenuated and attenuated marine pile driving. In *The Effects of Noise on Aquatic Life*; Springer: New York, NY, USA, 2012; pp. 439–444.
20. Bossanyi, E.A. The design of closed loop controllers for wind turbines. *Wind Energy* **2000**, *3*, 149–163. [[CrossRef](#)]
21. Bossanyi, E.A.; Fleming, P.A.; Wright, A.D. Validation of individual pitch control by field tests on two- and three-bladed wind turbines. *IEEE Trans. Control. Syst. Technol.* **2013**, *21*, 1067–1078. [[CrossRef](#)]
22. Bossanyi, E.A. Further load reduction with Individual pitch control. *Wind Energy* **2005**, *8*, 481–485. [[CrossRef](#)]
23. Kress, C.; Chokani, N.; Abhari, R.S. Downwind wind turbine yaw stability and performance. *Renew Energy* **2015**, *83*, 1157e65. [[CrossRef](#)]
24. Frau, E.; Kress, C.; Chokani, N.; Abhari, R.S. Comparison of performance and unsteady loads of multimegawatt downwind and upwind turbines. *J. Sol. Energ. Eng.* **2015**, *137*, 041004. [[CrossRef](#)]
25. He, K.; Qi, L.; Zheng, L.; Chen, Y. Combined pitch and trailing edge flap control for load mitigation of wind turbines. *Energies* **2018**, *11*, 2519. [[CrossRef](#)]
26. Maldonado, V. Active Flow Control of Wind Turbine Blades. In *Wind Turbines—Design, Control and Applications*; In-Tech: Rijeka, Croatia, 2016; pp. 303–324.
27. Stammer, M.; Thomas, P.; Reuter, A.; Schwack, F.; Poll, G. Effect of load reduction mechanisms on loads and blade bearing movements of wind turbines. *Wind Energy* **2019**, *23*, 274–290. [[CrossRef](#)]
28. Larsen, T.J.; Hanson, T.D. A method to avoid negative damped low frequent tower vibrations for a floating, pitch controlled wind turbine. *J. Phys. Conf. Ser.* **2007**, *75*, 012073. [[CrossRef](#)]
29. Bossanyi, E.A. Wind Turbine Control for Load Reduction. *Wind Energy* **2003**, *6*, 229–244. [[CrossRef](#)]
30. Johnson, K.; Pao, L.; Balas, M.; Fingersh, L. Standard and Adaptive Techniques for Maximizing Energy Capture. *IEEE Control. Syst. Mag.* **2006**, *26*, 70–81.

31. Laks, J.; Pao, L.Y.; Simley, E.; Wright, A.D.; Kelley, N.; Jonkman, B. Model Predictive Control Using Preview Measurements from LIDAR. In Proceedings of the 49th AIAA Aerospace Sciences Meeting including the New Horizons Forum and Aerospace Exposition, Orlando, FL, USA, 4–7 January 2011.
32. Dunne, F.; Simley, E.; Pao, L.Y. *LIDAR Wind Speed Measurement Analysis and Feed-Forward Blade Pitch Control for Load Mitigation in Wind Turbines*; National Renewable Energy Laboratory: Golden, CO, USA, 2011.
33. Bossanyi, E.A. Individual blade pitch control for load reduction. *Wind Energy* **2003**, *6*, 119–128. [[CrossRef](#)]
34. Muhando, E.; Senjyu, T.; Omine, E.; Funabashi, T.; Chul-Hwan, K. Functional Modeling for Intelligent Controller Design for MW-Class Variable Speed WECS with Independent Blade Pitch. In Proceedings of the 2nd Power and Energy, Johor Bahru, Malaysia, 1–3 December 2008; pp. 413–418.
35. Fischer, B. Reducing rotor speed variations of floating wind turbines by compensation of non-minimum phase zeros. In Proceedings of the EWEA, Lyon, France, 2–3 July 2012; pp. 144–147.
36. Jonkman, J. Influence of Control on the Pitch Damping of a Floating Wind Turbine. In Proceedings of the ASME Wind Energy Symposium, Reno, Nevada, 7–10 January 2008.
37. Fleming, P.; Pineda, I.; Rossetti, M.; Wright, A.; Arora, D. Evaluating Methods for Control Of An Offshore Floating Turbine. In Proceedings of the ASME 33rd International Conference on Ocean, Offshore and Arctic Engineering, San Francisco, CA, USA, 8–13 June 2014.
38. Luhmann, B.; Cheng, P.W. Relevance of aerodynamic modelling for load reduction control strategies of two-bladed wind turbines. *J. Phys.* **2014**, *524*, 012049. [[CrossRef](#)]
39. Sang, L.Q.; Maeda, T.; Kamada, Y.; Li, Q. Experimental investigation of the cyclic pitch control on a horizontal axis wind turbine in diagonal inflow wind condition. *Energy* **2017**, *134*, 269–278. [[CrossRef](#)]
40. Fleming, P.; Peiffer, A.; Schlipf, D. Wind Turbine Controller to Mitigate Structural Loads on A Floating Wind Turbine Platform. In Proceedings of the ASME 35th International Conference on Ocean, Offshore and Arctic Engineering, Busan, Republic of Korea, 19–24 June 2016.
41. Namik, H. Individual Blade Pitch and Disturbance Accommodating Control of Floating Offshore Wind Turbines. Ph.D. Thesis, University of Auckland, Auckland, New Zealand, 2012.
42. Skogestad, S.; Postlethwaite, I. *Multivariable Feedback Control: Analysis and Design*; John Wiley and Sons: Chichester, UK, 2007.
43. Maeda, T.; Kamada, Y.; Murata, J. LDV measurement of boundary layer on rotating blade surface in wind tunnel. *J. Phys. Conf. Series.* **2014**, *555*, 012057. [[CrossRef](#)]
44. Li, Q.; Murata, J.; Endo, M.; Maeda, T.; Kamada, Y. Experimental and numerical investigation of the effect of turbulent inflow on a Horizontal Axis Wind Turbine (Part I: Power performance). *Energy* **2016**, *113*, 713–722. [[CrossRef](#)]
45. Sang, L.Q.; Murata, J.; Morimoto, M.; Kamada, Y.; Maeda, T. Experimental investigation of load fluctuation on horizontal axis wind turbine for extreme wind direction change. *J. Fluid Sci. Technol.* **2017**, *12*, JFST0005. [[CrossRef](#)]
46. Tinnapob, P. Study on Three-Dimensional Flows in the Vicinity of the Horizontal Axis Wind Turbine Blade. Ph.D. Thesis, Mie University, Tsu, Japan, 2016.

Disclaimer/Publisher’s Note: The statements, opinions and data contained in all publications are solely those of the individual author(s) and contributor(s) and not of MDPI and/or the editor(s). MDPI and/or the editor(s) disclaim responsibility for any injury to people or property resulting from any ideas, methods, instructions or products referred to in the content.